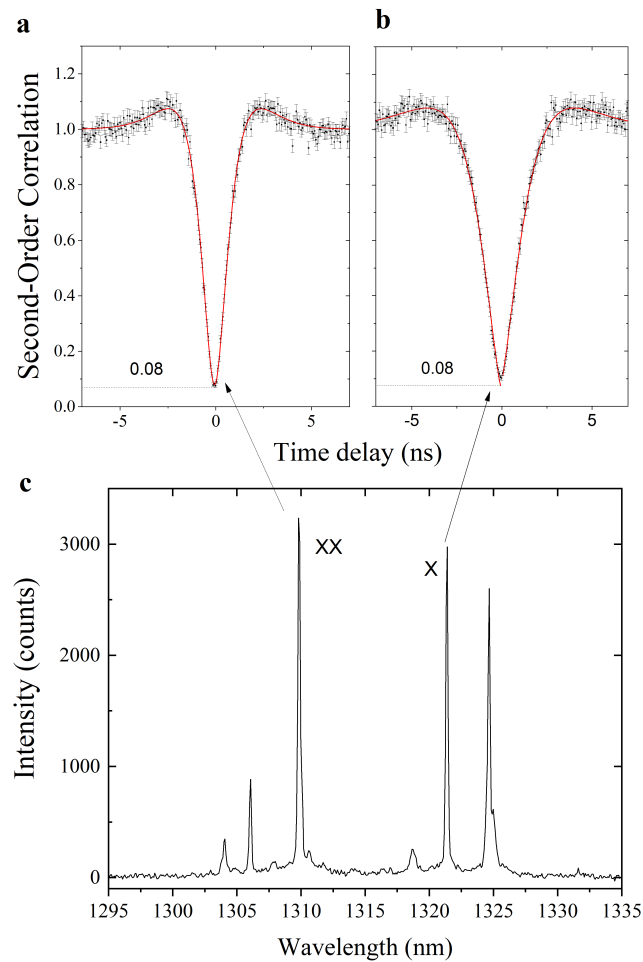


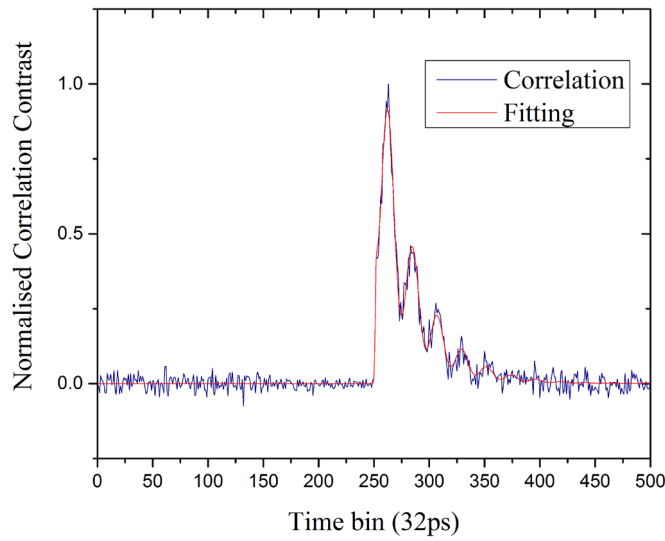
Supplementary Information

Supplementary Figures



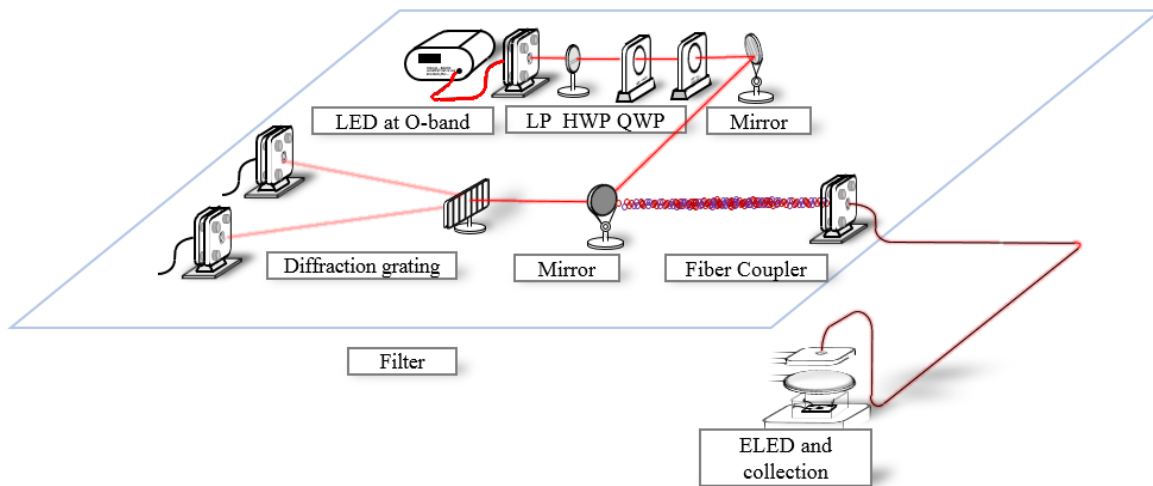
Supplementary Figure 1: Single photon emission.

Measurement of second order correlation function for **a** XX and **b** X photons including numerical fit. Displayed error bars are propagated from Poissonian counting statistics. **c** Spectrum of quantum dot for -2.6V bias voltage applied to tuning diode. The exposure time was 2s.



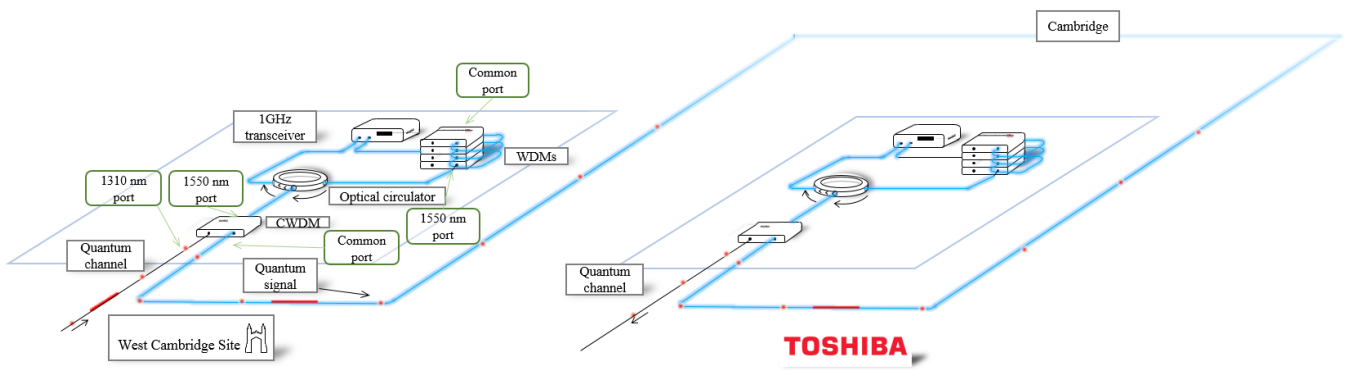
Supplementary Figure 2: Polarisation correlation in random detection basis.

Normalised difference of co- and cross-polarised photon coincidences measured in a random detection basis. The red curve shows an experimental fit according to equation (2) for extraction of the fine structure splitting and angular information of the detector basis orientation.



Supplementary Figure 3: Spectral filter and calibration module.

Experimental setup for injection of polarisation reference to qubit measurement system. Light from a broadband light-emitting diode (LED) in the telecom O-band passes a linear polariser (LP), a half wave plate (HWP) and a quarter wave plate (QWP) to generate arbitrary controllable polarisation reference states at X and XX wavelength.



Supplementary Figure 4: Wavelength multiplexing module.

Experimental setup for multiplexing of classical and quantum optical signals over the first installed fiber. WDM: Coarse Wavelength Division Multiplexer.

Supplementary Note 1

Efficient on-chip excitation

For comparison of the new optimized devices with conventional on-chip optically excited quantum dot (QD) emitters^{S1}, we have fabricated devices with the same mesa design on a wafer with similar layer structure but without the dedicated optical pump and absorption layer. Furthermore, these devices contain InAs QDs emitting at short wavelength around 900nm, with a matching weak distributed Bragg reflector (DBR) cavity. However, the difference in operating wavelength should be of no relevance for the following investigation. Most importantly, optical pumping light in these devices is emitted and absorbed in the wetting layer that has a thickness of less than 1nm. The emission wavelength of pumping light is around 870nm.

To assess the difference in optical excitation efficiency between the two different types of devices, we compared the intensity of pumping light emitted in the vertical direction from the pumping diode and from the tuning diode using a confocal microscope setup and spectrometer. On the pumping diode, this light originates from electrical injection and on the tuning diode it is generated from optical excitation and subsequent recombination of charge carriers in the absorbing 2D-layer containing the QDs. Therefore, the ratio of both spectral signals should be proportional to the absorption efficiency of pump light.

For the devices with only wetting layer pumping, we observe a ratio of 5.8 between emission from the pumping diode and emission from the tuning diode. For the telecom devices with 5nm pump and absorption layer, this ratio is reduced to 1.5, indicating an enhancement of the efficiency for on-chip optical excitation by almost a factor of 4. These observations are consistent with typical operating currents for the pumping diode required to saturate QD emission, being up to 10 times higher for devices with only wetting layer pumping. We understand these observations as a direct effect of less efficient photon absorption in the tuning diode due to the smaller thickness of the absorbing layer.

Supplementary Note 2

Single photon emission

An important feature of QD based entangled photon-pair sources is their single photon purity. Supplementary Figure 1 shows a spectrum of the ELED emission for operation conditions as used for the entanglement distribution experiment. The displayed second-order correlation ($g^{(2)}$) measurements for X and XX emission taken in a laboratory environment show strong anti-bunching for both photons of the entangled pairs, confirming that this is a single entangled-photon-pair source. The weak signal bunching observed in both measurements is indicative for dynamics involving more than only two levels. This is commonly explained by the presence of dark states which do non-radiatively couple to the excited state. The measurements are fitted with the following equation, taking the presence of up to four levels into account^{S2}.

$$g^{(2)}(x) = 1 + \frac{-(1 + A + B)e^{-\frac{|x-t_0|}{\tau_1}} + Ae^{-\frac{|x-t_0|}{\tau_2}} + Be^{-\frac{|x-t_0|}{\tau_3}}}{(1 + bg)^2}$$

$\tau_{1,2,3}$ and constants A and B represent the time constants and relative amplitudes of different decay channels. bg is the background to single photon ratio corresponding to the fraction of uncorrelated multiphoton events. From the measurement for the XX photons we extract a $g^{(2)}(0)$ value of 0.08 and a background to single photon ratio of 4.2%. As detector dark counts are negligible for photon rates measured in the laboratory, we associate this background with residual multi-photon emission from the source caused by leakage of photons from neighbouring spectral lines through the optical filter. For the corresponding $g^{(2)}$ measurement taken over the installed fiber as shown in the main text (Figure 4), we extract a background to single photon ratio of 15.4%. This can be understood as the sum of the background from the source (4.2%) and an additional

background (7.1%) due to a reduced signal caused by photon losses. The remaining contribution of 4.1% is most likely caused by stray light coupling into the photon collection at the remote location and small leakage from classical data traffic over the same fiber.

Supplementary Note 3

Classical-quantum multiplexing system

Supplementary Figure 4 shows the experimental setup which is used to multiplex classical data traffic with the transmission of entangled XX photons over installed fiber. The classical communication is established with standard 1550nm 1Gbit transceiver modules. Optical signals for inbound and outbound data traffic are routed by use of optical circulators at each end. The spectrum of the laser output for each transceiver is cleaned with a stack of 4 standard coarse wavelength division multiplexer (WDM) filters to suppress leakage of classical light into the telecom O-band. It is further attenuated to a launch power of $7.3\mu\text{W}$. Classical traffic and the quantum signal are wavelength-multiplexed by means of another WDM at each end. To further minimize leakage of classical signals into the qubit detection setup, we have introduced an additional free-space spectral filter at 1310nm (full width at half maximum (FWHM) $< 0.5\text{nm}$, not shown in the figure) which is installed after the multiplexing module at the Cambridge Research Laboratory.

Supplementary Methods

Measurement of fine structure splitting and alignment of detection basis

The evaluation of the entanglement fidelity from the QD source is typically done by correlation measurements in the horizontal/vertical (HV), diagonal/anti-diagonal (DA) and right-/left-handed circular (RL) bases in the reference frame of the eigenbasis of QD emission. Therefore, a precise alignment of the measurement setup to the eigenbasis of the QD emitter is essential. Conventional alignment methods make use of a calibrated reference that is injected into the main optical path towards the detectors, before the entangled photons are being coupled into the first optical fiber^{S3} as birefringence would otherwise rotate the linear (HV) eigenstates into unknown elliptical states. However, this configuration is usually bulky and not compatible with a compact collection setup as in this work, which only consists of a single collection lens (NA=0.5) and a fiber collimator outside of the cryostat window. We therefore developed a precise technique for detection of the QD eigenbasis after photons have propagated through birefringent media such as single mode fiber. This enables the injection of the correct polarisation references for detection calibration at an arbitrary point between the source and detectors.

The method works as follows. We take X-XX correlation measurements (co- and cross-polarised) in three well-known arbitrary but linearly independent detection bases in the reference frame of the polarisation reference. As will be explained in the following paragraphs, the time-dependent evolution of the correlation signal is then used to extract the exact orientation of each of the three reference states in the reference frame of the eigenbasis of QD emission. Using the standard procedure for Müller matrix evaluation, this allows us to calculate the transformation matrix between polarisation reference and QD eigenbasis which enables the generation of perfectly matching reference states for detector calibration in the second step.

The experimental setup is shown in Supplementary Figure 3, corresponding to the spectral filter module shown in Figure 3 in the main text. Entangled photons from the ELED are coupled into single mode fiber which guides them to the spectral filter module which is mounted in a separate instrument rack a few meters apart. A flip mirror is installed just before the diffraction grating in the filter, which is used to switch between the transmission of entangled photon pairs from the ELED and injection of a polarisation reference beam into the main optical path.

For a QD with fine structure splitting δ , the emitted entangled state has a time-dependent phase variation that can be described by the following equation:

$$|\varphi\rangle = |H_X\rangle|H_{XX}\rangle + e^{i\frac{\delta}{\hbar}t}|V_X\rangle|V_{XX}\rangle$$

Where $|P_X\rangle$ and $|P_{XX}\rangle$ represents polarisation state $|P\rangle$ in the eigenbasis of QD emission for X and XX photon, respectively. Let us assume that the detection system is aligned for projection to a randomly oriented polarisation state $|H'\rangle$ described by the parameters θ and φ in spherical coordinates on the Poincaré sphere:

$$|H'\rangle = \cos\frac{\theta}{2}|H\rangle + \sin\frac{\theta}{2}e^{i\varphi}|V\rangle$$

Projection of XX photons to $|H'\rangle$ will collapse the exciton photon into state

$$|P'_X\rangle = \langle H'_{XX} | \varphi \rangle = \cos\frac{\theta}{2}|H_X\rangle + \sin\frac{\theta}{2}e^{i(\frac{\delta}{\hbar}t - \varphi)}|V_X\rangle.$$

The probability for the detection of a co-polarized coincidence between X and XX photons is then described by

$$p_{co} = |\langle P'_X | H' \rangle|^2 = 1 - 2 \sin^2\frac{\theta}{2} \cos^2\frac{\theta}{2} (1 - \cos(\frac{\delta}{\hbar}t - 2\varphi)). \quad (1)$$

Experimentally, we measure co- and cross-polarised photon coincidences c_{PP} and c_{PQ} and calculate the normalised difference $d_{PQ} = A(c_{PP} - c_{PQ})$ with A being a normalization constant (see Supplementary Figure 2). This relates then to equation (1) as

$$d_{PQ} = (2 p_{co} - 1) \times e^{-t/\tau} \quad (2)$$

where τ is a constant accounting for exponential decay of the photon correlation due to the natural lifetime of the X state and other spin dephasing processes including repumping. A numerical fit to experimental two-photon correlations in a certain detection basis therefore enables the extraction of precise values for the fine structure splitting δ and for angles θ and φ . The relation between these angles and the corresponding Stokes parameters s_1, s_2, s_3 is given by

$$\begin{aligned} s_1 &= \cos\theta \\ s_2 &= \sin\theta \cos\varphi \\ s_3 &= \sin\theta \sin\varphi. \end{aligned}$$

The polarisation transformation of an optical fiber or other linear optical elements is conveniently described by the Müller matrix \mathbf{M} .

$$\mathbf{S}_m = \mathbf{M} \cdot \mathbf{S}_r$$

Where \mathbf{S}_r is the Stokes vector for the orientation of the polarisation detection system, being calibrated by a corresponding reference state. \mathbf{S}_m is the Stokes vector extracted from fitting equation (2) to photon pair correlations, which describes the orientation of the QD eigenbasis with respect to the calibration reference state. It is straight forward to reconstruct \mathbf{M} from a set of calibration states (e.g. $\mathbf{S}_r \in \{\mathbf{H}, \mathbf{D}, \mathbf{R}\}$) and their corresponding measured vectors \mathbf{S}_m ^{S4}. Knowledge of \mathbf{M} then enables deterministic setting of reference calibration states \mathbf{S}_r , that perfectly match the principal polarisation states \mathbf{S}_{eigen} in the reference frame of the QD emitter

$$\mathbf{S}_{r'} = \mathbf{M}^{-1} \cdot \mathbf{S}_{eigen}.$$

Supplementary references

- S1. Lee, J. P. *et al.* Electrically driven and electrically tunable quantum light sources. *Applied Physics Letters* **110**, 71102 (2017).
- S2. Anderson, M. *et al.* Quantum teleportation using highly coherent emission from telecom C-band quantum dots. *npj Quantum Inf* **6**, 1023; 10.1038/s41534-020-0249-5 (2020).
- S3. Young, R. J. *et al.* Improved fidelity of triggered entangled photons from single quantum dots. *New Journal of Physics* **8**, 29 (2006).
- S4. Layden, D., Wood, M. F.G. & Vitkin, I. A. Optimum selection of input polarization states in determining the sample Mueller matrix: a dual photoelastic polarimeter approach. *Optics express* **20**, 20466–20481 (2012).